Clays and Clay Minerals, Vol. 50, No. 3, 314–330, 2002.

IN SITU CHARACTERIZATION AND DIFFERENTIATION OF KAOLINITES IN LATERITIC WEATHERING PROFILES USING INFRARED MICROSPECTROSCOPY

ANICET BEAUVAIS[1,*] AND JACQUES BERTAUX[2]

[1] Cerege-IRD, UR-037, Europôle Méditerranéen de l'Arbois, B.P. 80, 13545 Aix-en-Provence Cedex, France
[2] IRD, UR-055, Centre d'Ile de France, LFS, 32 avenue Henri Varagnat, 93143 Bondy Cedex, France

Abstract—Lateritic weathering kaolinites have been characterized *in situ* and differentiated for the first time by means of infrared microspectroscopy (IRMS). Four classical OH-stretching bands have been observed in the Fourier transform infrared (FTIR) spectra, at 3695, 3668, 3650 and 3620 cm^{-1}, denoted ν_1, ν_2, ν_3 and ν_4, respectively, plus a band at 3595 cm^{-1} associated with the octahedral substitution of Fe^{3+} for Al^{3+}. Infrared microspectroscopy of thin-sections of lateritic weathering profiles provides useful information on the types of kaolinite present in different horizons of the profile. The spectra obtained from large well-ordered kaolinite crystals look like those obtained by diffuse reflectance in that, compared with the KBr disk spectra of <2 μm powders, bands at 3668 and 3650 cm^{-1} are enhanced, and the strong absorption of KBr disks at 3695 cm^{-1} is replaced by a broad weaker band from 3700–3680 cm^{-1}. In laterites, these large well-ordered kaolinites often exhibit a band at 3595 cm^{-1} indicative of significant Fe^{3+} substitution for Al^{3+} in the structure. The IR microspectra obtained from regions of small, more poorly-ordered kaolinites do not differ so markedly from that of KBr disks. All show enhanced absorption around 3650 cm^{-1} compared with well-ordered kaolinites, indicating that the disorder is due, at least in part, to domains of dickite-like and/or nacrite-like stacking in their structure. The 3595 cm^{-1} band is always weaker than that of the well-ordered kaolinite in the same profile. The IRMS data from well-characterized reference kaolinites show that the ratio $A\nu_2/A\nu_3$ is a pertinent IR order index for kaolinites. The larger this index, the larger is the area of the 3595 cm^{-1} band, and the larger and the more ordered is the kaolinite sample. It is suggested that the diversity of FTIR spectra observed reflects intergrowths of kaolinite-dickite polymorphs, or at least mixtures of high- and low-defect kaolinites which are frequently encountered in the lateritic geosphere rather than pure kaolinitic phases. The largest kaolinites having secondary crystallized in voids are the most ordered and the most ferruginous and have been considered as useful mineralogical tracers of the recent evolution of old lateritic terrains.

Key Words—Dickite, Infrared Microspectroscopy, Kaolinite, Lateritic Weathering, Longitudinal Optical Mode, Structural Order, Transverse Optical Mode

INTRODUCTION

Kaolinite is a ubiquitous clay mineral in lateritic weathering profiles developed at the expense of many kinds of parent rocks in tropical areas (Millot, 1970; Murray, 1988). The crystal chemistry of kaolinite is, however, very complex. For instance, it has been shown that its structural order index depended on defect centers and substitution of Fe^{3+} for Al^{3+} in the octahedral sites, and that these reflected various geochemical conditions of the medium in which it crystallized (Hinckley, 1963; Angel *et al.*, 1974; Jones *et al.*, 1974; Meads and Malden, 1975; Rengasamy, 1976; Mendelovici *et al.*, 1979; Mestdagh *et al.*, 1980, 1982; Cases *et al.*, 1982; Brindley *et al.*, 1986; Giese, 1988; Muller and Calas, 1989; Muller *et al.*, 1995). Different generations of kaolinite and kaolin polymorphs characterized by their own crystal chemical properties may effectively develop in the same weathering profile according to specific structural and textural patterns (Cantinolle *et al.*, 1984; Ambrosi and Nahon, 1986; Muller and Bocquier, 1987; Nahon, 1991). It has long been accepted that weathering matrices with inherited parent-rock structure generally contain well-crystallized kaolinite with low Fe substitution, while clayey matrices with blurred parent-rock structure embed poorly-crystallized kaolinite with higher Fe substitution (Herbillon, 1980; Didier *et al.*, 1983; Cantinolle *et al.*, 1984; Muller and Bocquier, 1987). The aim of this work is to characterize *in situ* different types of standard kaolinite along with kaolinites of lateritic origin on polished thin-sections by means of the infrared microspectroscopy (IRMS), and to try relating the crystal chemical characteristics of the second ones to the geochemical conditions of the medium in which they crystallized.

Background

In past decades, numerous studies made progress in understanding the relations between the kaolinite structure and its infrared (IR) spectroscopic signatures. Pertinent data in the mid-IR range were obtained especially in the region of the OH-stretching vibrations, *i.e.* between 3550 and 3750 cm^{-1}. Indeed, OH bands are very sensitive probes for distinguishing between kaolin clay minerals and for determining their structure

* E-mail address of corresponding author:
beauvais@arbois.cerege. fr

(Farmer, 1964, 1974, 1998, 2000; Farmer and Russell, 1964; Ledoux and White, 1964; Parker, 1969; Rouxhet *et al.*, 1977; Cruz-Cumplido *et al.*, 1982; Brindley *et al.*, 1986; Prost *et al.*, 1989; Johnston *et al.*, 1990; Frost and Van der Gaast, 1997). As the kaolinite unit-cell contains only four different OH groups (Bish, 1993), the IR spectra of kaolinites obviously exhibit four OH-stretching bands at frequencies of 3695, 3668, 3650 and 3620 cm^{-1}, which were denoted ν_1, ν_2, ν_3 and ν_4, respectively (Farmer 1998; Frost and Johansson, 1998). The three higher frequency bands, ν_1, ν_2 and ν_3, have been assigned to the three inner-surface hydroxyls on the layer surface, here termed the OuOH groups, while ν_4 at ~3620 cm^{-1} stands for the inner hydroxyls, *i.e.* the InOH groups (Ledoux and White, 1964; Rouxhet *et al.*, 1977; Johnston *et al.*, 1990). Another OH-stretching band denoted ν_5 was also designated near 3685 cm^{-1} by using Raman spectroscopy (Wiewióra *et al.*, 1979; Johnston *et al.*, 1985; Frost and Van der Gaast, 1997; Farmer, 1998). The occurrence of the 3685 cm^{-1} band was recently ascribed to a transverse optical (TO) vibration involving the in-phase stretching vibration of the three inner-surface hydroxyls in the unit-cell. This vibration gives rise to ν_1 at 3695 cm^{-1} in KBr disk spectra (Farmer, 1998, 2000). The bands resulting from the vibration of the OuOH groups, including ν_5, are generally attributed to coupled in-phase and out-of-phase inner surface hydroxyls (Rouxhet *et al.*, 1977; Brindley *et al.*, 1986; Frost and Van der Gaast, 1997; Farmer, 1998).

Empirical tests from XRD and IR spectroscopy analyses have long been applied to assess the crystallinity of kaolinite; after Brindley *et al.* (1986), we will use structural order or disorder rather than good or poor crystallinity. For instance, the hydroxyls absorption patterns of kaolinites have been shown to reflect the degree of structural disorder (Barrios *et al.*, 1977; Prost *et al.*, 1989). Among them, the ratio between the integrated intensity, *i.e.* the area, of OH-stretching bands at 3668 cm^{-1} and 3650 cm^{-1} empirically documents the structural order or disorder of kaolinite (Farmer, 1974; Mestdagh *et al.*, 1982; Brindley *et al.*, 1986). An IR spectrum of a poorly-ordered kaolinite effectively presents a poorly-resolved ν_2 OH-stretching band. Brindley *et al.* (1986) showed that the wavenumber of ν_1 decreased with the width at half-height of ν_4 as the structural order measured by the Hinckley index increased. On the basis of Rietveld refined structural data, this finding was, however, questioned (Plançon *et al.*, 1988, 1989). Farmer and Russell (1964) and Prost *et al.* (1989) argued that IR spectra of poorly-crystallized kaolinites revealed the existence of dickite- and nacrite-like configurations whose proportion increased with increasing structural disorder.

Most previous IR spectroscopic techniques required the mechanical extraction of clay fractions, but this is not the best way to distinguish clay minerals according to their various sizes and morphologies. What one generally analyzes with classical transmission IR on KBr powder pellets of weathering materials is a mixture of well-ordered and poorly-ordered small-size kaolinites. It has been also suggested that pressing kaolinite particles when making KBr pellets had an effect on the intensities of the OH-stretching bands (Bell *et al.*, 1991), that is avoided when using IRMS. The advantage of IRMS is its ability to analyze a limited zone in a thin-section, selecting either single flakes of kaolinite 'booklets' or a population of optically similar small kaolinites. Soil scientists make much use of thin-sections to describe soil profiles, and the recent development of IR microscopes makes it possible to measure a spot as small as 20 µm either in transmission or in reflection mode. Very few studies, however, have explored the capacity of the IRMS technique for the *in situ* characterization of clays in soils. Rintoul and Fredericks (1995) used reflection-mode IRMS for studying bauxitic pisoliths. Johnston *et al.* (1990) obtained indirect information on the OH structure of single crystals of dickite and kaolinite using a polarizing IR microspectrometer. They showed that the intensities of the 3620 and 3668 cm^{-1} bands were influenced by rotation of the electrical vector around the *c* axis in the *ab* plane of a single crystal of kaolinite, whereas the intensity of the 3650 cm^{-1} band was not changed. They concluded that all OuOH are oriented almost perpendicular to the octahedral sheet, while the InOH are sub-parallel to the sheets, pointing at the octahedral vacancy, later confirmed by Farmer (1998, 2000). We present new insights on the application of IRMS in transmission mode for the *in situ* characterization of different types of kaolinites in thin-sections. We believe that IRMS is a suitable technique for studying the hydroxyl region of kaolinites from lateritic soil profiles even with large amounts of Fe oxyhydroxides.

MATERIALS AND TECHNIQUE

Samples

Kaolinites from reference standards and from tropical soils were investigated *in situ* in thin-sections by IRMS. The reference samples are of different origins and exhibit varying size and structural order (Table 1). Two specimens of well-ordered hydrothermal kaolinites, DCV, a pure sample (Allard, 1994) and GB1, from France and Great Britain, respectively; five sedimentary kaolinites, among them, two well-ordered samples, A1, from Manaus in Brazil and, KGa1, from Georgia in the USA, and three more disordered samples, KGa2, FU7 and FBT2, from Georgia in the USA and France, respectively; and one soil kaolinite, B4, from Manaus in Brazil (Table 1). Soil kaolinites were also analyzed from samples collected in three lateritic weathering profiles belonging to the same topographical sequence in south-eastern Central African Republic (Figure 1). Detailed petrological and geochemical studies of the profiles have been reported (Beauvais, 1991, 1999; Beauvais and

https://doi.org/10.1346/00098600260358076 Published online by Cambridge University Press

Table 1. Characterization of kaolinite specimens.

Sample	Reference or source	Location	R2	E_{120K}
(1) A1 <20 μm	Lucas *et al*., 1987	Manaus (b) Brazil	0.7	9.3
(2) DCV >2μm	Gaite *et al*., 1993	Aveyron (a) France	1.35	3.1
(3) GB1	Cases *et al*., 1982	Cornwall (a) Great Britain	1.13	6.2
(4) KGa1	van Olphen and Fripiat 1979	Georgia (b) USA	1.03	6.2
(5) KGa2	van Olphen and Fripiat 1979	Georgia (b) USA	0.69	10
(6) FU7	Cases *et al*., 1982	Charentes (b) France	0.23	14
(7) FBT2 <38 μm	Delineau *et al*., 1994	Charentes (b) France	0.44	14.2
(8) B4 <20 μm	Lucas *et al*., 1987	Manaus (c) Brazil	0.23	12.6

Numbers in parentheses refer to the spectra of Figures 5 and 6
(a) hydrothermal; (b) sediment; (c) soil.
R2 = XRD disorder index of Liétard (Cases *et al*., 1982)
E_{120K} = EPR disorder index measured at 120 K (Gaite *et al*., 1997; Balan *et al*., 1999)

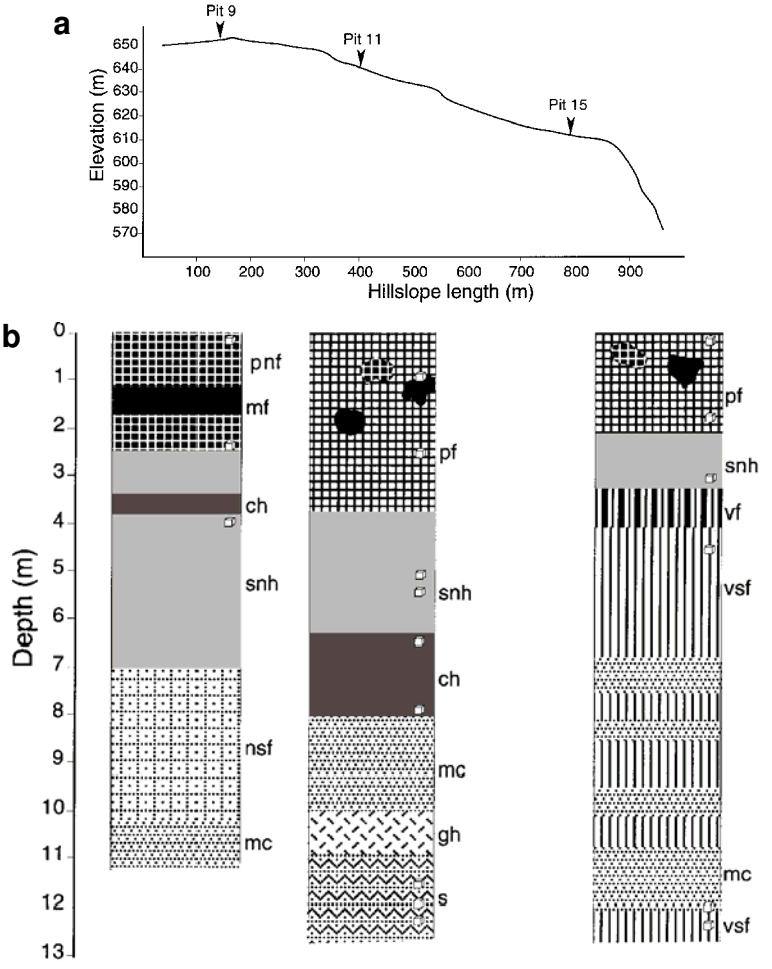

Figure 1. (a) Topographic location of the lateritic weathering profiles in which kaolinites were analyzed by IRMS. (b) Descriptive sketch of the profiles in the Central African Republic (the small cubes represent samples in which thin polished sections have been made for the IRMS analysis; s = saprolite; gh = gibbsitic horizon; mc = mottled clays; ch = clayey horizon; snh = soft nodular horizon; nsf = nodular soft ferricrete; vsf = vermiform soft ferricrete; vf = vermiform ferricrete; mf = massive ferricrete; mnf = metanodular ferricrete; pf = protopisolitic ferricrete). The different ferricrete facies were defined by Tardy (1993).

https://doi.org/10.1346/00098600260358076 Published online by Cambridge University Press

Colin, 1993). From the bottom to the top of the profiles, five standard horizons were observed, a saprolite, a mottled clayey horizon, a soft nodular horizon, a soft ferricrete and a ferricrete (Figure 1). Notice that the ferricrete is geochemically degraded and progressively replaced by micronodular soft soils wherever the forest is developing (Beauvais and Tardy, 1991). The soft nodular horizons contain lithorelic nodules with the parent-rock structure, and pedorelic nodules with a soil structure as previously described by Beauvais (1991). Kaolinite was analyzed in each horizon. It is associated with goethite, hematite and gibbsite in various proportions depending on the horizon facies, *i.e.* the location in the profiles (Figure 1b). In saprolite, ferruginous nodules and ferricrete matrices with preserved parent-rock structure, the kaolinite platelets of 10–20 μm are stacked as 'booklets' of 40–50 μm in size accross the *c* axis (Figure 2). The making of thin-sections thus leads to a variety of kaolinite 'booklets' orientations according to the three crystallographic axes, *a*, *b*, *c*. In all the profile horizons except the saprolite, the kaolinites of crypto-crystalline clay-ferruginous matrices without parent-rock structure, are smaller, 1–2 μm in size (Figure 3). These two kinds of kaolinite are supposed to have different crystal chemical characteristics reflecting different geochemical properties of the medium in which they have been formed.

Experimental procedure

Well-characterized reference kaolinites were first analyzed using KBr pellets. The samples were ground mechanically with small agate balls in an agate vial under acetone and in a refrigerated area at 4°C in order to prevent heating and structural changes of particles. A particle size <2 μm was required to avoid excessive scattering of IR radiation. The powder was carefully mixed by hand with KBr in an agate mortar. A dilution of 0.25% was used for all samples studied. Weighing was done within a dry atmosphere, with an accuracy of 10^{-5} g. A 300 mg pellet, 13 mm in diameter, was prepared by pressing the mixture in a vacuum die, with up to 8 tons cm^{-2} of compression. The pellets were oven dried for two days at 110°C before data acquisition.

Transmission Fourier transform IR (FTIR) spectra of these KBr pellets were recorded at room temperature on a Perkin-Elmer FT 16 PC spectrometer in the 4000–250 cm^{-1} energy range with a 2 cm^{-1} resolution. The beam crossing the KBr pellet has an approximate diameter of 8 mm, so that this method can be considered as IR macrospectrometry in relation to the IR microspectrometry technique described below. For each spectrum, 50 scans were cumulated. Absorbance was computed relative to a background of sample holder containing a pure KBr pellet.

Infrared absorption spectra of kaolinites from thin-sections were obtained by transmission at room temperature. The spectra were recorded with a Bruker A 590 microscope coupled with an equinox 55 Bruker FTIR spectrometer in the frequency range 6000–1500 cm^{-1}.

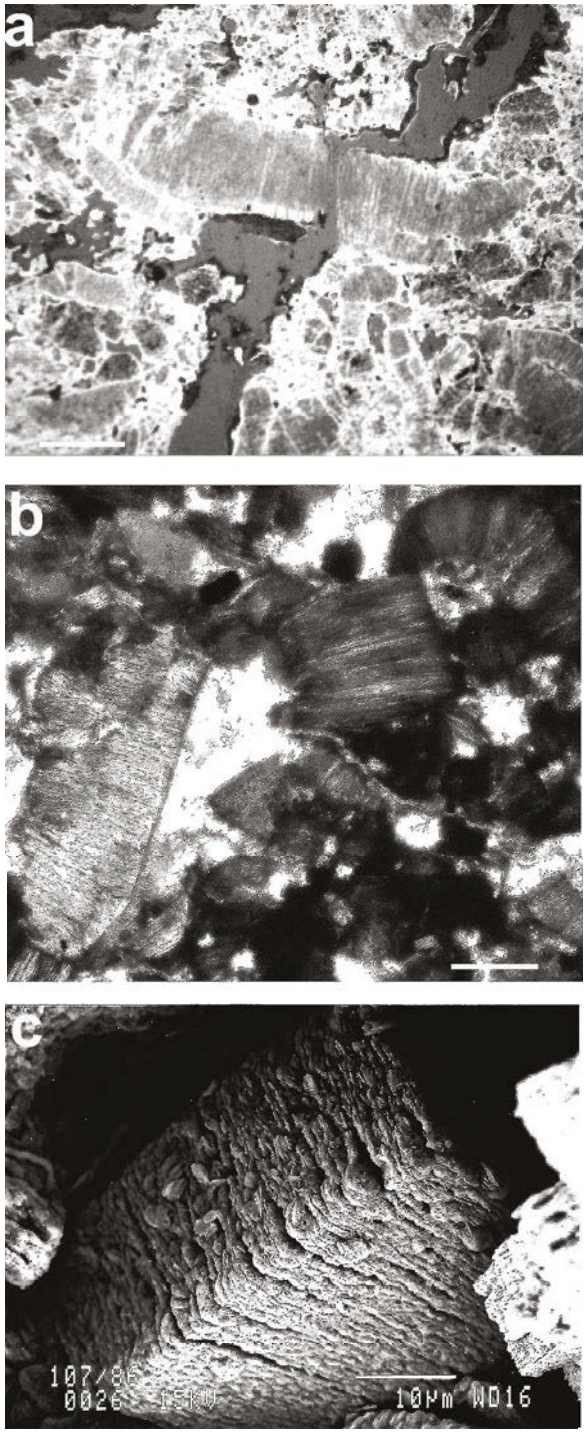

Figure 2. Large secondary kaolinite 'booklets' crystallized in large voids of ferruginous matrices of nodules and ferricrete. (a) Under reflected light optical microscope (scale bar = 10 μm). (b) Under polarized optical microscope and partially replaced by gibbsite crystals (scale bar = 5 μm). (c) Under scanning electron microscope coated by iron oxyhydroxides (scale bar = 10 μm).

https://doi.org/10.1346/00098600260358076 Published online by Cambridge University Press

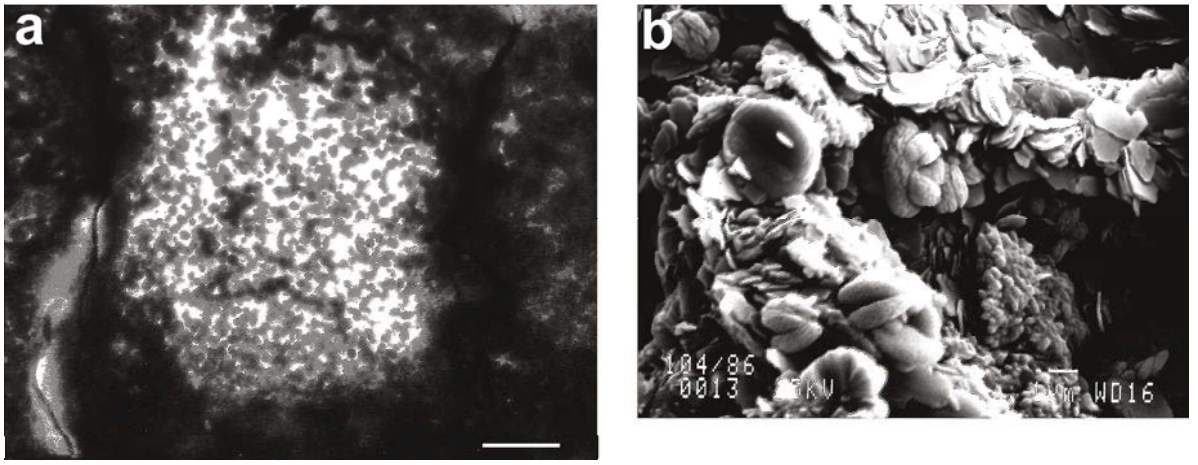

Figure 3. Small-size kaolinites associated with micronodular hematite in nodules and ferricrete of the high plateau profile. (a) Viewed under polarized optical microscope (scale bar = 5 μm). (b) Under scanning electron microscope (scale bar = 1 μm). Note the small hexagonal flakes of well-crystallized kaolinite and the 'doughnut' habit of hematite, these latter corresponding to several coalesced micronodules of hematite in Figure 3a.

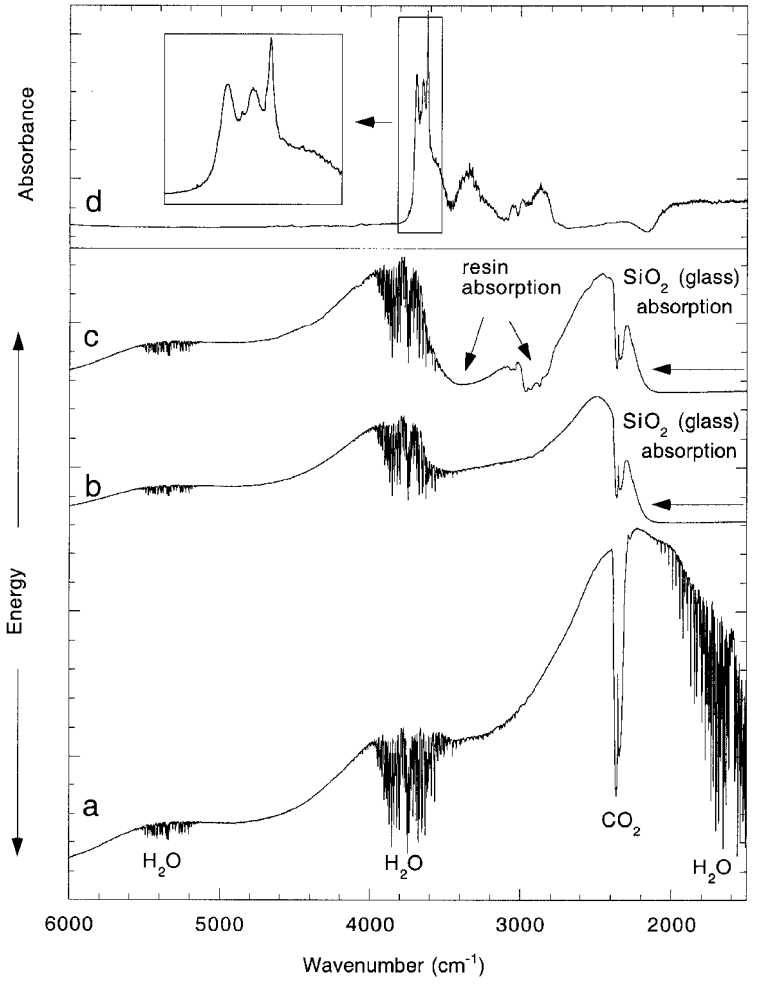

Figure 4. IR microspectrometry transmission measurements through a thin-section. a, b and c are single-channel measurements through a 50 μm spot of air, glass slide and glass slide plus resin, respectively. The resulting curves show the variation of energy in arbitrary unit *vs*. wavelength given as its inverse, the wavenumber. The narrow absorption bands due to atmospheric H_2O and CO_2 are shown in curve a. d is the IRMS spectrum of clays in a thin-section of soil, with an enlargement of the OH-stretching region.

https://doi.org/10.1346/00098600260358076 Published online by Cambridge University Press

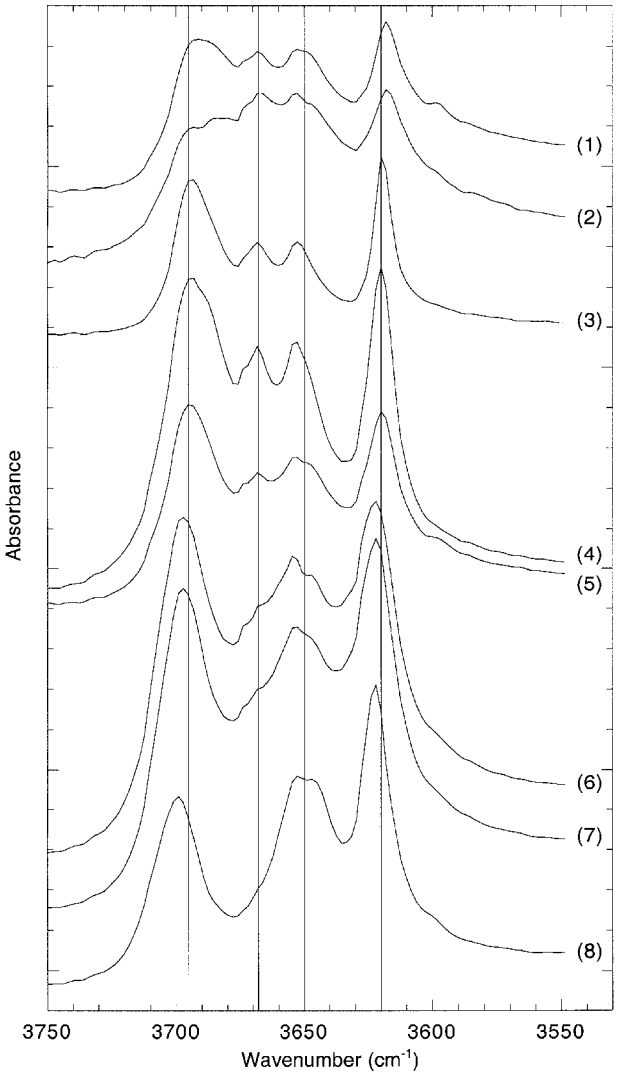

Figure 5. IRMS spectra of the well-characterized reference kaolinites in thin-sections. The numbers refer to sample numbers in Table 1. The vertical lines represent the standard centered absorption-band positions of well-ordered kaolinites, ν_1 at 3695 cm^{-1}, ν_2 at 3668 cm^{-1}, ν_3 at 3650 cm^{-1} and ν_4 at 3620 cm^{-1}.

This configuration used a Globar source and a liquid N_2-cooled narrow-band mercury-cadmium telluride (MCT) detector to optimize the response in the OH-stretching region (Johnston *et al*., 1990). The beam size was reduced to a diameter of 50 μm, *i.e.* an area of 1962.5 μm^2 was analyzed which includes several kaolinite flakes in the case of 'booklets' (Figure 2), or a mixture of numerous smaller kaolinites, $\leqslant 2$ μm, with Fe oxyhydroxides in the case of clay-ferruginous matrices (Figure 3). Preliminary test measurements were made with a spectral resolution at 2 or at 4 cm^{-1}, and the co-addition of 300 or 100 scans, respectively. As no significant changes in absorption band characteristics were detected, the spectra were recorded by the accumulation of 100 scans at a resolution of 4 cm^{-1}. The aperture of the microscope is either filled with the (110), (010) or (110) faces of the kaolinite crystals stacked as 'booklets' along the *c* axis that results from different cut planes used to make the thin-sections (Figure 2). Although we did not use a polarization system, perhaps we should consider that the resulting different orientations of the kaolinite 'booklets' to the incident IR beam could give rise to variations in intensities of the OH-stretching bands, similar to those observed when applying a polarization system (Johnston *et al*., 1990, 1998). Kaolinite books with different orientations regarding the *c* axis also result in various Raman spectra (Frost and Van der Gaast, 1997). Unfortunately, we do not have any means to accurately determine the orientations of 'booklets' in the thin-sections.

The *in situ* measurements were made on soil thin-sections, 30 μm thick, mounted, after impregnation with resin, on a glass slide and subsequently polished. Glass slides, *i.e.* amorphous silicate, are transparent to the IR

https://doi.org/10.1346/00098600260358076 Published online by Cambridge University Press

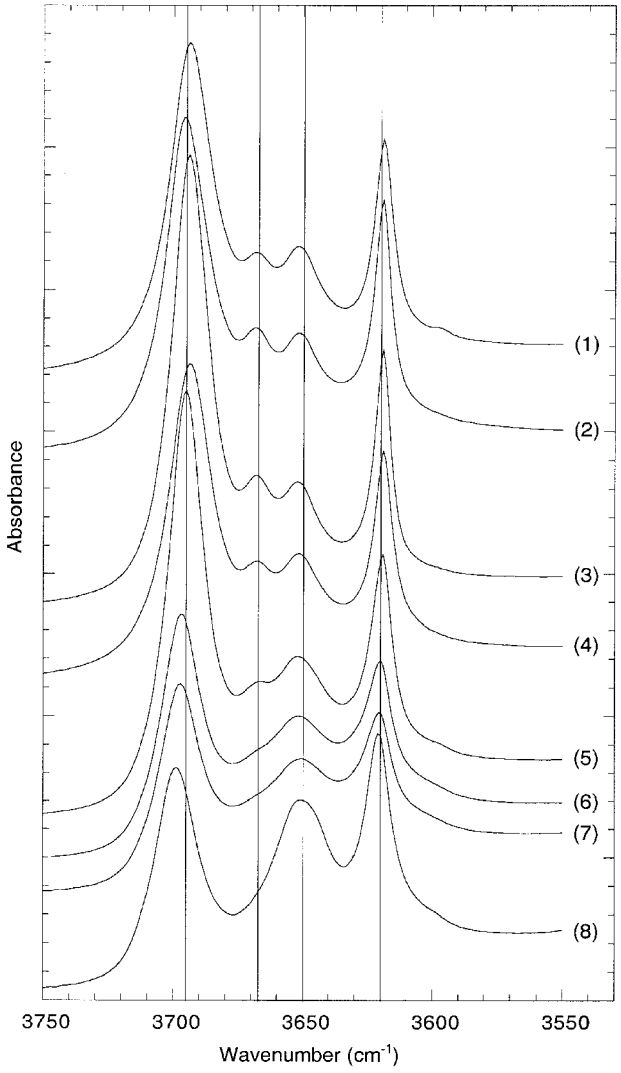

Figure 6. IR spectra of the well-characterized reference kaolinites in KBr pellets (numbers and vertical lines as in Figure 5).

radiation above 2500 cm^{-1}, where no absorption due to SiO_4 tetrahedra occurs; this still allows a thorough observation of the OH region between 3500 and 3800 cm^{-1} (Figure 4). The level of energy received by the MCT detector when no thin-section is crossed allows the measurement of IR absorption between 6000 and 1500 cm^{-1} (Figure 4a), with a maximum of energy, *i.e.* best signal to noise ratio, between 1500 and 2500 cm^{-1}. The glass slide absorbs all the energy below 2200 cm^{-1} (Figure 4b), while additional absorption due to the resin of the thin-section occurs around 2800–3000 cm^{-1} and as a broad band centered at 3400 cm^{-1} (Figure 4c). Finally, the only remaining energy available for a measurement through a thin-section lies between 2250 and 2750 cm^{-1} and above a frequency of 3500 cm^{-1} over which the OH-stretching vibrations of clays absorb the IR radiation, so that the spectra have been expanded between 3570 and 3750 cm^{-1} (Figure 4d). All transmission-absorption spectra measured on thin-sections were referenced against a measurement of the absorption solely due to the glass slide and the epoxy resin used to make the thin-sections (Figure 4c).

The baseline of each IR and IRMS spectrum was corrected by using the interactive mode of the Bruker OPUS software, meaning that a third-order polynomial was applied; after which, the envelopes of the identified OH-absorption bands were decomposed into Lorentzian components. Experimental and calculated spectra were fitted by a least-squares procedure using the Marquardt-Levenberg algorithm (Marquardt, 1963). The band component analyses were based on the objective observation of four to five absorption bands in each spectrum and on the best resulting RMS error, which was generally $\leqslant 0.05$. The area of each band was calculated as a percentage of the total OH-stretching area between 3550 and 3750 cm^{-1}.

https://doi.org/10.1346/00098600260358076 Published online by Cambridge University Press

Table 2. Location and description of kaolinite samples in the high plateau profile (P9) analyzed by IRMS.

Sample	Horizon (depth)	Texture description
104-2n (1)	Soft nodular (4 m)	Light yellow internodular clay-ferruginous matrix
104-1 (2)	as above	Orange clay-ferruginous plasma in a pedorelict ferruginous nodule
104-12 (3)	as above	Orange clay-ferruginous internodular matrix
104-11 (4)	as above	Kaolinite 'booklet' within a hematitic lithorelict nodule (see Figure 7c)
104-5 (5)	as above	as above
104-4 (6)	as above	as above
107_4 (1)	Ferricrete (2.5 m)	yellow cryptocrystalline internodular matrix (see Figure 8c)
107_10 (2)	as above	as above
107-0n (3)	as above	Clay-ferruginous matrix within a lithorelict nodule
107-3 (4)	as above	Orange matrix within a nodule (see Figure 8c,d)
107_29 (5)	as above	as above
107_8 (6)	as above	Secondary kaolinite 'booklet' within a hematitic nodule (see Figure 2)
107_2 (7)	as above	White kaolinite 'booklet' within a lithorelict nodule (see Figure 7d)
107_1 (8)	as above	Kaolinite 'booklet' coated by orange ferruginous oxy-hydroxides within a lithorelict nodule (see Figure 7e,f)
107_7 (9)	as above	Small size kaolinite coated with micronodular hematite (see Figures 3 and 8a)
110-0 (1)	Ferricrete (0.10 m)	Small-size kaolinite within a pedorelict nodule
110-1 (2)	as above	Small-size kaolinite within a nodule's yellow rim (see Figure 8b)
110-2n (3)	as above	as above
110-10 (4)	as above	Mixture of 'booklets' and small size kaolinites
110-8 (5)	as above	Kaolinite 'booklet' within a lithorelict nodule
110-11 (6)	as above	as above
110-7 (7)	as above	as above
110-13 (8)	as above	Kaolinite with inherited mica structure (see Figure 8b)

Numbers in parentheses refer to spectra in Figure 10a–c

RESULTS AND DISCUSSION

Kaolinites from standard references

Kaolinites from well-characterized standard references (Table 1) have been analyzed in thin-section by IRMS. The resulting spectra of relatively well-ordered, (1) to (4), and disordered, (5) to (8), kaolinites are presented in Figure 5 and compared to those obtained with IR spectroscopy on KBr pellets (Figure 6). Four classical absorption bands at 3695, 3668, 3650 and 3620 cm^{-1}, *i.e.* ν_1, ν_2, ν_3 and ν_4, respectively, are observed (Figures 5 and 6). Additional weaker bands are, however, also detected, at 3685 and 3645 cm^{-1}, plus a pair of very weak frequencies around 3670 cm^{-1} in the

Table 3. Location and description of kaolinite samples in the upslope profile (P11) analyzed by IRMS.

Sample	Horizon facies (depth)	Texture description
186-1 (1)	Saprolite (12 m)	Small size kaolinite with goethite
186-2 (2)	as above	as above
19-1 (3)	Saprolite (11.5 m)	as above
17-0 (4)	as above	Kaolinitic plasma with booklets (see Figure 7b)
17_3 (5)	as above	Kaolinite booklets
17_5 (6)	as above	Mixture of large and small size kaolinites (see Figure 7a)
17_6 (7)	as above	Kaolinitic plasma with smaller size kaolinite
17_7B (8)	as above	kaolinite 'booklet'
27-3 (3)	Mottled clays (8 m)	Red clay-ferruginous plasma
31-1 (1)	as above	
61-1 (2)	Soft nodular (5 m)	Pink clay matrix
33-6 (4)	Idem (5.5 m)	Clay-ferruginous matrix embedding nodules
33-8 (5)	as above	Ferruginous nodule
33-9 (6)	as above	as above
69-2 (1)	Ferricrete (1 m)	Orange-brown matrix embedding nodules
66-1 (2)	as above (2.5 m)	Clay-ferruginous matrix embedding nodules
69-1 (3)	as above (1 m)	Clay-ferruginous yellowish plasma
66-4 (4)	as above (2.5 m)	Clay-ferruginous matrix embedding nodules
66-2 (5)	as above	Clay plasma within a nodule

Numbers in parentheses refer to spectra of Figure 9a–c

https://doi.org/10.1346/00098600260358076 Published online by Cambridge University Press

Table 4. Location and description of kaolinite samples in the downslope profile (P15) analyzed by IRMS.

Sample	Horizon facies (depth)	Texture description
78-0 (1)	Soft ferricrete (12.5 m)	Yellow rim around a black nodular domain
79-2 (2)	Mottled clays (12 m)	White crypto-crystalline clayey plasma (see Figure 8e)
79-5 (3)	as above	as above
85 (4)	Soft ferricrete (8.6 m)	Orange clay-ferruginous matrix
91-2 (5)	as above (4.5 m)	White-yellowish clay matrix
94-4 (7)	Soft nodular (3.05 m)	Red-orange plasma at the edge of void crossing the matrix
96-9 (8)	Ferricrete (2.05 m)	Yellow clay matrix
96-10 (9)	as above	Orange clay-ferruginous plasma in a pedorelict nodule
96-6 (11)	as above	Kaolinite booklet
96-13 (12)	as above	as above
96-15 (13)	as above	Many kaolinite booklets
100-0 (6)	Ferricrete (0.10 m)	Yellow clay-ferruginous matrix embedding hematitic nodules (see Figure 8f)
100-13 (10)	as above	Small size kaolinite coated with micronodular hematite within a pedorelict nodule
100-9 (14)	as above	Kaolinite inside a hematitic nodule

numbers in parentheses refer to spectra of Figure 11

IRMS spectra (Figure 5). According to V.C. Farmer (pers. comm.), these can result from diffusely scattered and/or specularly reflected radiations entering the spectrometer because of the wide angles of convergence and divergence of the incident and collected radiations, respectively. It is a characteristic of reflectance spectra that weak absorption bands are enhanced, whereas strong absorption bands are replaced by a region of high reflectivity extending from the transverse to the longitudinal frequencies (Farmer, 2000); *e.g.* from 3685 to 3697 cm^{-1}. From the well-ordered to the disordered kaolinite, one observes on both figures, a shift of ν_1 and ν_4 to higher wavenumbers, and an aditional weak absorption band at ~3597 cm^{-1} in spectra (1), (2), (5) and (8), of samples A1, DCV, KGa2 and B4, respectively (Figures 5 and 6). That latter band results from Al-Fe substitution in the octahedra of the kaolinite structure, and can be denoted as ν_{Fe}. Spectrum (8) of B4 is almost like a spectrum of dickite, with only three absorption bands, the first being centered at ~3700 cm^{-1}. This could support the idea that a poorly-ordered kaolinite would be an intergrowth of kaolinite- and dickite-like structures (Farmer and Russell, 1964; Barrios *et al.*, 1977; Lombardi *et al.*, 1987; Prost *et al.*, 1989). The resemblance between the IR and IRMS spectra (Figures 5 and 6) has motivated the application of the IRMS technique to kaolinite samples of soil thin-sections.

Kaolinites of lateritic weathering profiles

Lateritic weathering kaolinites have been examined in each petrographical facies of three different vertical profiles, as described above (Figure 1; Tables 2–4). Two kinds of kaolinite were analyzed using IRMS: large (10–20 μm) crystals stacked as 'booklets' in saprolite (Figure 7a,b), and also in lithorelic ferruginous nodules, (either as secondary crystallizations or intimately associated with Fe oxyhydroxides (Figures 2, 7c–f)); and small ($\leqslant 2$ μm) randomly-oriented kaolinites in crypto-crystalline clay-ferruginous matrices inside or around ferruginous nodules (Figures 3, 8a to d and 8f), or also in illuviated gray-white clay deposits filling large elongate voids looking like 'socks' (Figure 8e). These two types of kaolinite were observed throughout the three profiles, from the saprolite to the ferricrete, within the clay-ferruginous matrices and the nodules (Tables 2 to 4); and they have been distinguished according to their respective IRMS spectrum (Figures 9 to 11). In Figures 9 to 11, examples of spectra are presented for the different kaolinite crystal sizes of different weathering facies in upslope (pit 11), high plateau (pit 9) and downslope (pit 15) profiles (Figure 1). The numerous IRMS spectra presented account for the diversity of clay textures observed in the thin-sections (Tables 2–4; Figures 2, 3, 7 and 8).

Examination of the different spectra in the OH-stretching region ranging from 3550 to 3750 cm^{-1} reveals the four classical bands represented by vertical straight lines in Figures 9 to 11, which correspond to the four well-known OH-stretching bands, ν_1, ν_2, ν_3 and ν_4 at ~3695, 3668, 3650 and 3620 cm^{-1}, respectively. As already noted, weak absorptions ascribed to TO mode are also observed (Figures 9 to 11). These bands will not be considered in the curve-fitting procedure. In the following, some representative types of large-size and small-size kaolinites are described with their respective FTIR spectrum in the OH-stretching region ranging from 3550 to 3750 cm^{-1}.

Large-size kaolinites. Kaolinites from the saprolite of the upslope profile, P11, derive from the pseudomorphic weathering of parent minerals like amphiboles, plagio-

https://doi.org/10.1346/00098600260358076 Published online by Cambridge University Press

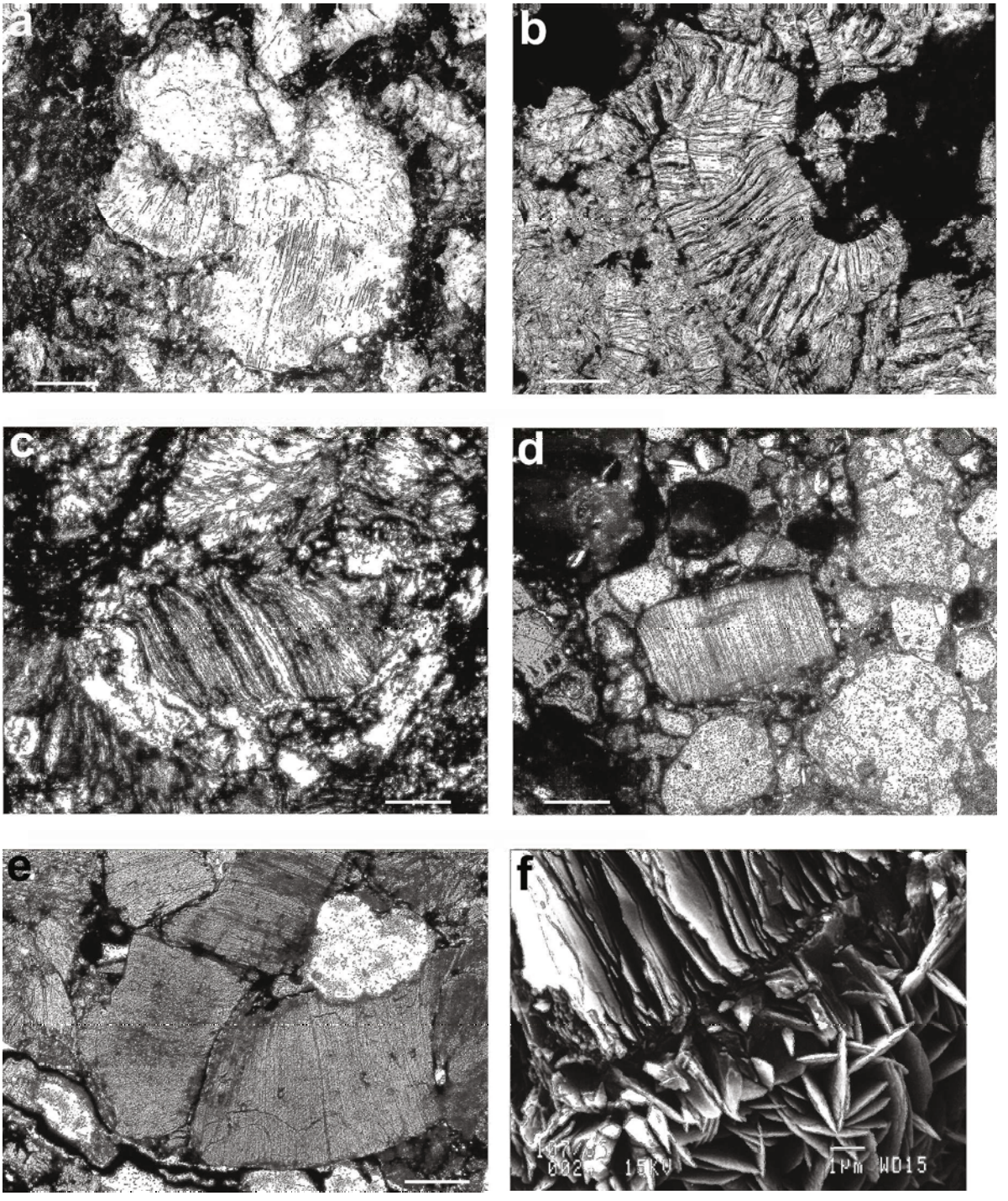

Figure 7. Large-size well-crystallized kaolinites: (a) and (b) in the saprolite of the upslope profile (scale bar = 10 µm); (c) in the soft nodular horizon with more or less ferruginous coatings (scale bar = 5 µm); (d) and (e) in the ferricrete of the high plateau profile (scale bar = 10 µm). (a) to (e) Polarized optical micrographs and (f) scanning electron micrograph of kaolinite 'booklets' coated by goethite crystals in the ferricrete of the high plateau profile (scale bar = 1 µm).

clases, chlorites, epidotes and phengites (Beauvais, 1999). Although the volume of parent minerals is preserved, the kaolinites may have different sizes and morphologies (Figure 7a,b) and exhibit different IRMS spectra labeled 4 and 6 for the larger ones and 3 for the smaller ones in Figure 9a. The spectra labeled 4, 5 and 6 in Figure 10a correspond to large-size kaolinite 'booklets' inside lithorelic nodules of the soft nodular horizon of the high plateau profile (Figure 10c). The large kaolinite 'booklets' of Figure 7d–f in the ferricrete of the high plateau

https://doi.org/10.1346/00098600260358076 Published online by Cambridge University Press

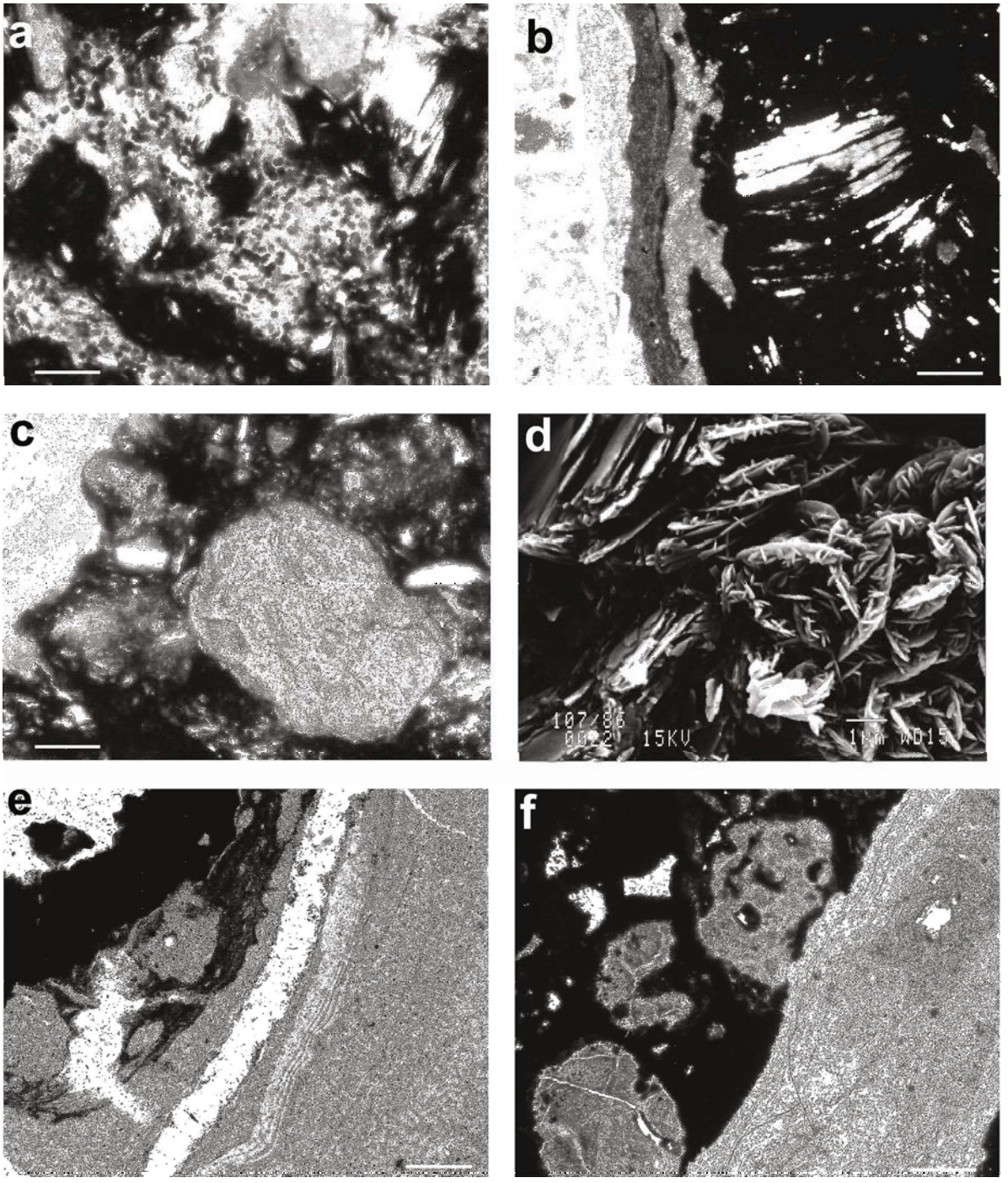

Figure 8. Small-size kaolinites in the ferricrete of the high plateau profile. (a) Well-crystallized, associated with micronodular hematite (scale bar = 5 µm). (b) Poorly-crystallized within yellow crypto-crystalline clay ferruginous matrices (lighter left part of the photomicrograph) around a ferruginous nodule containing a kaolinite 'booklet' with inherited micas structure (scale bar = 10 µm). (c) Within orange matrices in nodules (light gray in the center of the photomicrograph) (scale bar = 5 µm). (d) Scanning electron micrograph of small size kaolinites with goethite (scale bar = 1 µm). (e) In the downslope profile, poorly-crystallized kaolinite in illuviated clay material filling a large void in the soft ferricrete (scale bar = 10 µm). (f) In a yellow clay ferruginous matrix (light gray, right-hand side of the photomicrograph) enclosing a nodule of the ferricrete (scale bar = 10 µm).

profile exhibit spectra labeled 7 and 8 in Figure 10b, respectively, while the secondary kaolinite 'booklets' crystallized in voids (Figure 2) have a spectrum labeled 6 in Figure 10b. Large kaolinite with inherited mica structure (Figure 8b) in ferricrete at the top of the high plateau profile gives spectrum 8 in Figure 10c.

https://doi.org/10.1346/00098600260358076 Published online by Cambridge University Press

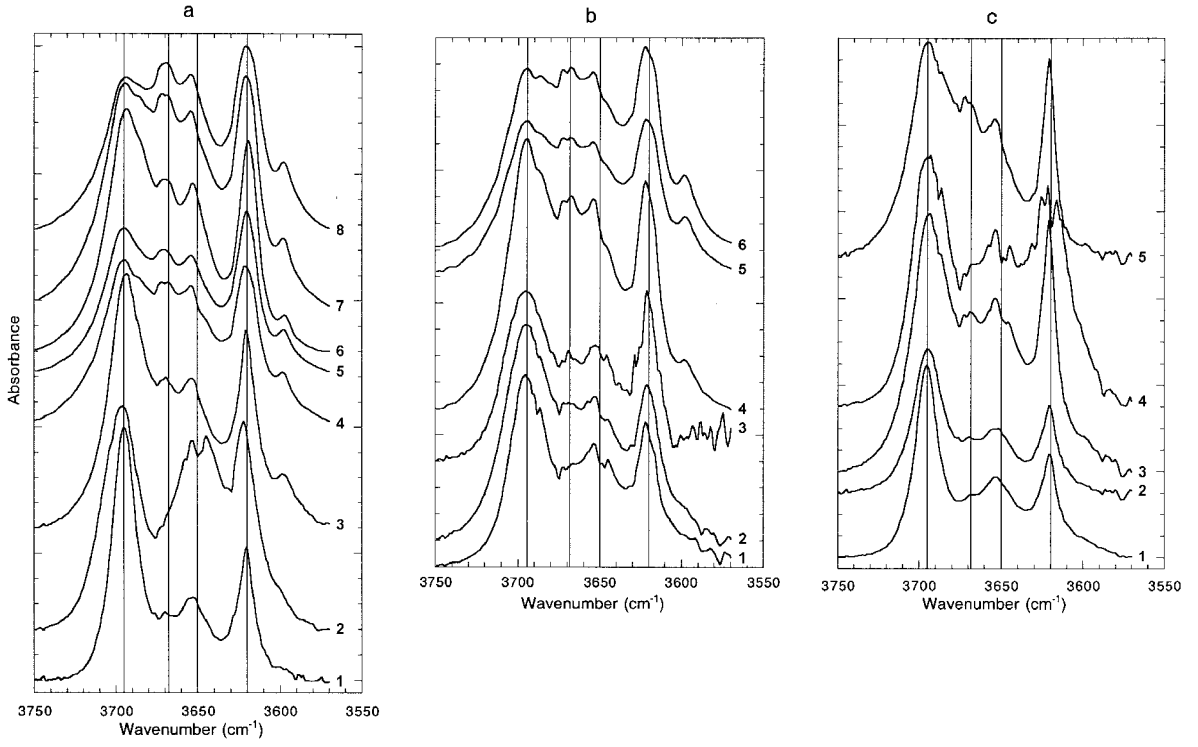

Figure 9. IRMS spectra of the two types of kaolinite in the upslope profile, pit 11; (a) in the saprolite horizon (1—3 = small-size kaolinites; 4—8 = large-size kaolinites); (b) in the mottled clays and soft nodular horizons (1—3 = small-size kaolinites; 4—6 = large-size kaolinites); (c) in the ferricrete horizon (1—4 = small-size kaolinites; 5 = large-size kaolinites). See Figure 5 for an explanation of the vertical lines.

Large-size kaolinites exhibit various IRMS spectra according to the differences in band intensities of the inner-surface hydroxyls (Figures 9—11). These are characterized by five bands, ν_2 standing for the 3668 cm^{-1} band is particularly well resolved. A band at ~3595 cm^{-1} assigned as ν_{Fe} has been also detected, reflecting structural Fe^{3+} substituting for Al^{3+}. The intensity of this well-known vibration band is generally in proportion to the Fe^{3+} substitution rate for Al^{3+} in octahedral sites of the kaolinite structure (Mestdagh *et al.*, 1980; Cases *et al.*, 1982; Delineau *et al.*, 1994). A frequency attributed to TO mode of the in-phase OH-stretching vibration also occurs at ~3685 cm^{-1}.

Small-size kaolinites. Small-size kaolinites associated with micronodular hematite in ferricrete of high plateau profiles (Figures 3 and 8a) give rise to spectrum 9 in Figure 10b. Small-size kaolinites of crypto-crystalline clay-ferruginous plasma inside nodules of ferricrete (Figure 8c) give spectrum 4 in Figure 10b. Ferruginous nodules of ferricretes are generally embedded into a crypto-crystalline yellow clay-ferruginous matrix (Figure 8b,c,f), the kaolinite of which is very small, $\leqslant 1$ μm. That kaolinite is characterized by IRMS spectra labeled 1 and 2 in Figure 10b, 2 in Figure 10c or 6 in Figure 11. Small-size kaolinites may also have been translocated by illuviation processes through large pores and voids of the soft ferricrete in the downslope profile. Such a clay material is typically oriented (Figure 8e) and has spectra labeled 2 or 3 in Figure 11.

Small-size kaolinites have spectra indicating they are poorly-ordered, with a good resolution of bands at 3700, 3654 and 3620 cm^{-1} but with ν_2 of large-size kaolinite being weak or absent. The band ν_{Fe} is commonly present but weaker than in spectra of large-size kaolinites (Figures 9—11). Some spectra also exhibit an additional band at ~3645 cm^{-1}. Such a frequency has been reported in Raman spectra of coarsely-crystalline dickite by Johnston *et al.* (1998). In the IRMS spectra of small poorly-ordered kaolinites, the bands at 3654 and 3645 cm^{-1} could arise from regions of dickite- and nacrite-like stacking, respectively (Farmer and Russell, 1964; Barrios *et al.*, 1977; Lombardi *et al.*, 1987; Prost *et al.*, 1989), or at least from the mixture of high- and low-defect kaolinites (Johansson *et al.*, 1998).

Before differentiating each kaolinite type by band area measurements, we should point to some obvious differences between the two types. From the small-size to the large-size kaolinites, there is an increasing intensity of the band at 3668 cm^{-1}, ν_2, a decreasing intensity of the band at 3695 cm^{-1}, ν_1, and the occurrence of a well-resolved band at ~3595 cm^{-1}, ν_{Fe}, this last band being very poorly expressed in the spectra of small-size kaolinites (Figures 9—11). Some

https://doi.org/10.1346/00098600260358076 Published online by Cambridge University Press

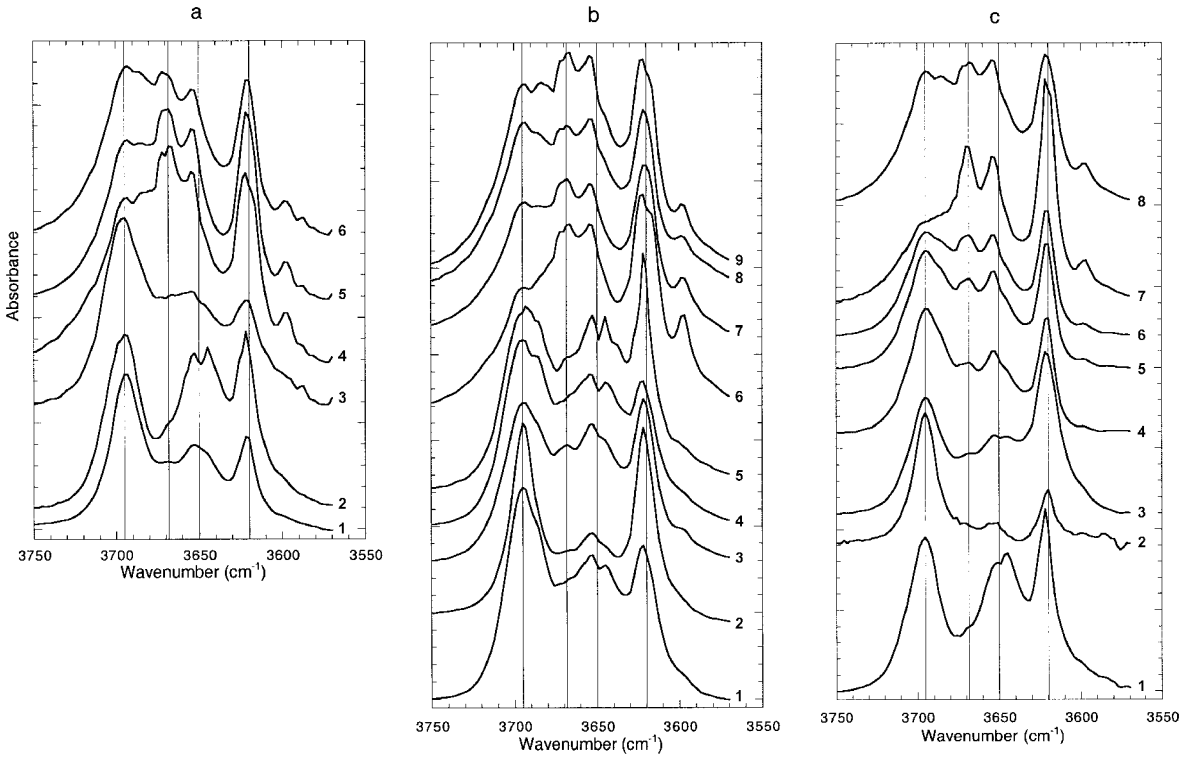

Figure 10. IRMS spectra of the two types of kaolinite in the high plateau profile, pit 9; (a) in the soft nodular horizon (1—3 = small-size kaolinites; 4—6 = large-size kaolinites); (b) at 2 m depth in the ferricrete horizon (1—5 = small-size kaolinites; 6—9 = large-size kaolinites); (c) at 0.10 m depth in the ferricrete horizon (1—4 = small-size kaolinites; 5—8 = large-size kaolinites). See Figure 5 for an explanation of the vertical lines.

large-size kaolinites also show a LO/TO pair in the 3668—3670 cm^{-1} region, while many small-size kaolinites exhibit a band at 3645 cm^{-1} near ν_3.

Large-size vs. small-size kaolinites. Only the significant linear relationships between the band areas have been examined to distinguish the large-size from the small-size kaolinites. Five bands were used for the decomposition, ν_1, ν_2, ν_3, ν_4 and ν_{Fe} when it was necessary. As ν_1, ν_2 and ν_3 in well-ordered kaolinites have been ascribed to coupled in-phase and out-of-phase inner surface hydroxyls (Rouxhet *et al.*, 1977; Frost and van der Gaast, 1997; Farmer, 1998), the relationships between the areas of these three absorption bands were examined. The plot of the area of ν_2, ($A\nu_2$), against the area of ν_1, ($A\nu_1$), discriminates the two groups of kaolinite, with the large-size kaolinites characterized by $15 < A\nu_2 < 31$ and $18 < A\nu_1 < 50$, while the small-size kaolinites have $4 < A\nu_2 < 18$ and $35 < A\nu_1 < 53$ (Figure 12).

The plot of the area of ν_2 against that of ν_3 also obviously discriminates large-size from small-size kaolinites around an area ratio of ν_2 over ν_3 equal 1 (Figure 13a). The area of the 3668 cm^{-1} band (ν_2) and more generally the ratio of the areas of ν_2 and ν_3 reflects the structural order-disorder of the kaolinite, *i.e.* $A\nu_2/A\nu_{3(\text{disordered kaolinites})} \leqslant 1 \leqslant A\nu_2/A\nu_{3(\text{ordered kaolinites})}$ (Cases *et al.*, 1982; Brindley *et al.*, 1986). This is confirmed by Figure 14, where the reference kaolinites exhibit good correlations between the disorder indexes R2 and E_{120K} given in the Table 1 and the ratio $A\nu_2/A\nu_3$, this effectively being a reliable IR order index for the kaolinites. Well-ordered kaolinites are characterized by the highest values of R2 and $A\nu_2/A\nu_3$, and the lowest E_{120K}, whereas the disordered kaolinites exhibit low R2, high E_{120K}, and low $A\nu_2/A\nu_3$ (Table 1, Figure 14). According to Figure 13b, large kaolinites are characterized by a ratio $A\nu_2/A\nu_3$ ranging from 0.81 to 1.84, while it averages ~0.5, ranging from 0.09 to 0.81, for small kaolinites (Figure 13b). This implies that large-size kaolinites are well ordered whereas most small-size kaolinites are rather disordered. Based on results obtained from IR spectroscopy on KBr pellets, it has, however, long been thought that the more structural defects a kaolinite contained, the more it incorporated octahedral Fe^{3+}, and thus, the more it was disordered (Mestdagh *et al.*, 1980; Cases *et al.*, 1982). Our results, however, show quite a different trend, with a significant positive correlation between the areas ratio $A\nu_2/A\nu_3$ and $A\nu_{Fe}$, the latter being larger for the large kaolinites than for the smaller ones (Figure 13b). This means that, under natural lateritic conditions, large-size kaolinites stacked as 'booklets' can crystallize in large voids from Fe-rich (Si, Al) solutions and have crystal chemical characteristics of

https://doi.org/10.1346/00098600260358076 Published online by Cambridge University Press

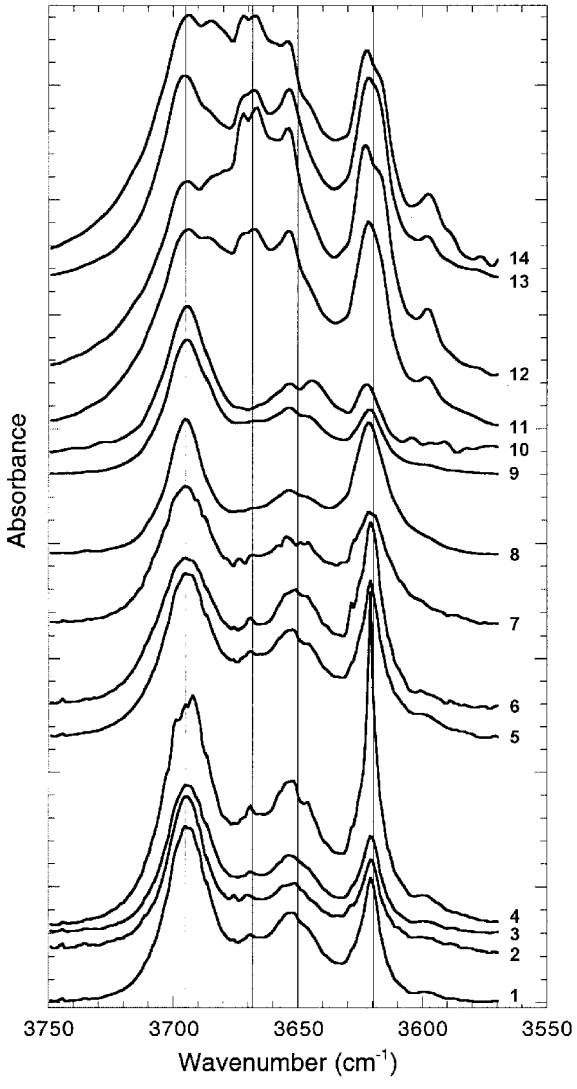

Figure 11. IRMS spectra of the two types of kaolinite from the mottled clays and the soft ferricrete at the bottom to the ferricrete horizon at the top of the downslope profile, pit 15 (1–10 = small-size kaolinites; 11–14 = large-size kaolinites). See Figure 5 for an explanation of the vertical lines).

well-ordered kaolinite, whereas small-size kaolinites can be poorly ordered and poor in Fe. These results show that the quantity of Fe in the octahedral structure of kaolinite is not simply related to the IR order index, $A\nu_2/A\nu_3$, and thus to the structural order of the kaolinite. Well-ordered kaolinites with structural Fe have been synthetized (Petit and Decarreau, 1990), and this is also consistent with the positive relation of $A\nu_2/A\nu_3$ to $A\nu_{Fe}$ (Figure 13b).

For small-size kaolinite, the areas of ν_2 and ν_{Fe} are not correlated, indicating that if these kaolinites are all the more disordered as the area of ν_2 is reduced, they can exhibit various amounts of Fe substitution for Al (Figure 13b). Low-defect or less-disordered kaolinites can incorporate large amounts of Fe, meaning that the relation between the octahedral substitution of Fe^{3+} for

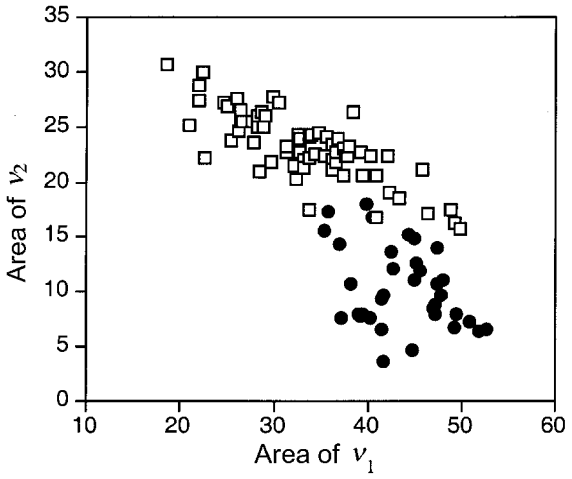

Figure 12. Relationships between the band intensities of the inner surface hydroxyls, $A\nu_2$ *vs.* $A\nu_1$ (open squares = kaolinite 'booklets'; filled circles = small-size kaolinites).

Al^{3+} and the proportion of structural defects and/or stacking faults is not as obvious as previously believed. Large-size and small-size kaolinites probably have different growth kinetics and thermodynamics that control the amount of structural defects on the one hand, and the amount of structural Fe on the other hand, without any simple relationship between one and the other.

To summarize, the two kaolinite groups have been clearly distinguished using band area measurements (Figures 12,13). The large-size kaolinites are all the more ordered as the areas of ν_2, ν_{Fe} and the ratio of the areas ν_2:ν_3 are all large. The crystal chemical characteristics of the best-ordered kaolinites agree well with the results published by Petit and Decarreau (1990) on Fe^{3+}-doped kaolinites obtained from synthesis products. The small-size kaolinites are all the more disordered as the area of ν_2 andν_{Fe} are low, and as the area of ν_1 and ν_3 are, on average, relatively higher than those of the large-size kaolinites (Figures 12,13a). No particular differences were found within the same group of kaolinites, large or small, according to the different horizons of the same weathering profile; this limits the interpretation of the results in terms of geochemical process signatures.

We have, however, noticed that, within the group of large-size kaolinite stacked as 'booklets', a majority of those exhibiting the highest $A\nu_2/A\nu_3$ and $A\nu_{Fe}$ (Figure 13b) have secondary crystals of gibbsite in large voids (Figure 2). This requires percolation of Fe-rich (Si, Al) solutions through the weathering profiles; such solutions are likely in a semi-humid wooded environment with high organic-matter contents (Beauvais and Tardy, 1991). Under such pedoclimatic conditions, the geochemical degradation of the upper ferruginous horizons, *i.e.* the ferricretes, effectively permits the partial release of Fe with Al and silica (Beauvais, 1999). It was recently suggested that the actual weathering profiles have undergone past pedoclimatic changes that could explain the variety of weath-

https://doi.org/10.1346/00098600260358076 Published online by Cambridge University Press

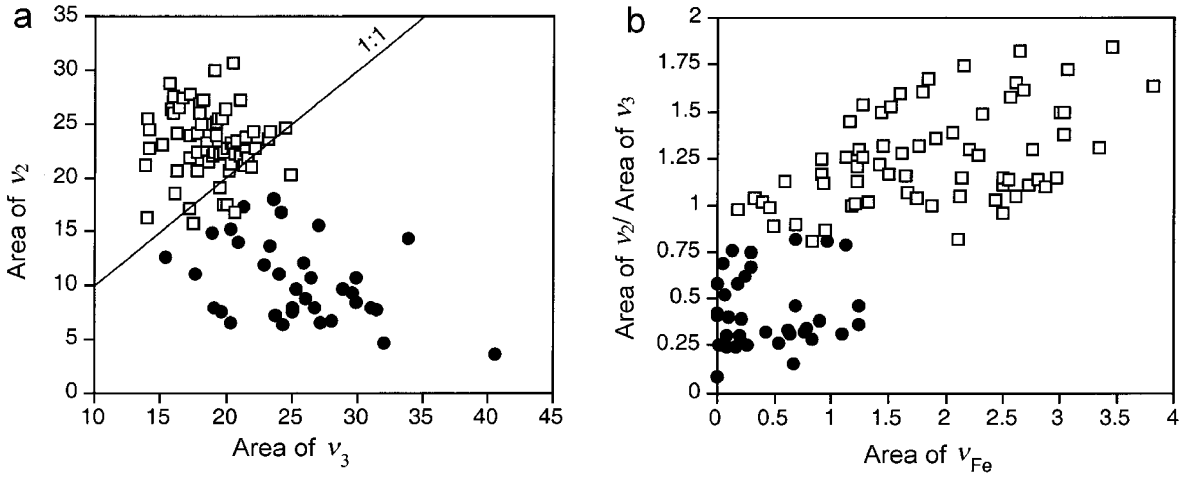

Figure 13. Relationships between the band intensities of the inner surface hydroxyls. (a) $A\nu_2$ *vs.* $A\nu_3$; the 1:1 straight line is for $A\nu_2 = A\nu_3$. (b) $A\nu_2/A\nu_3$ *vs.* $A\nu_{Fe}$ at 3595 cm^{-1} (see Figure 12 for an explanation of the symbols).

ering facies and kaolinites as well (Beauvais, 1999). No obvious crystal chemical differences have, however, been noted between the kaolinite 'booklets' of the saprolite and those observed in the nodules of the soft nodular horizon or in the hematitic matrices of the ferricrete. Our results mean that perhaps some kaolinite 'booklets' of the matrices of the upper ferruginous horizons could have been inherited from previous saprolitic materials (Beauvais, 1999), while the secondary kaolinite 'booklets' associated with gibbsite crystals in large voids crossing the primary structures could be good mineralogical tracers of the ferricrete degradation described earlier (Beauvais and Tardy, 1991; Beauvais, 1999). Further IRMS investigations would, however, be necessary to differentiate better the different types of kaolinite 'booklets', and to relate their OH absorption band patterns to specific geochemical processes.

CONCLUSIONS

Infrared microscopy is a valuable technique for measuring *in situ* the OH-absorption bands of selected kaolinites directly on soil thin-sections. Although the low frequencies of the IR spectrum of kaolinite are perturbed by the presence of glass, resin and glue used in preparing the thin-sections, the information contained in the OH-stretching region is of sufficient quality to distinguish different kinds of kaolinite. Contributions of this technique with respect to the KBr pellets method are (1) the *in situ* analysis of clay minerals within oriented undisturbed rock samples, and (2) the differentiation of well-ordered and poorly-ordered kaolinites according to their respective size and texture in the rock sample. The IRMS results show that the ratio of the integrated intensities of ν_2 at 3668 cm^{-1} over ν_3 at 3650 cm^{-1}, $A\nu_2/A\nu_3$, remains a good index of structural order for the kaolinites. Lateritic weathering kaolinites could be intergrowths of kaolinite- and dickite-like structures or at least mixtures of low- and high-defect kaolinites whether they are large or small, the relative contribution of which reflecting various geochemical, thermodynamic and/or growth kinetics conditions controlling the kaolinite formation. Clay mixtures are quite likely in the studied weathering profiles in which recent evolution can be traced from secondary kaolinite 'booklets', which are the best ordered and more ferruginous.

ACKNOWLEDGMENTS

This work is dedicated to the late Prof. Ph. Ildefonse. It is a contribution from IRD (UR 037 and UR055) and Cerege. Dr T. Allard and the LMC laboratory (University of Paris 6 and 7) are gratefully aknowledged for providing us with reference kaolinites. Dr V.C. Farmer and an anonymous referee are acknowledged for their useful critiques of a previous version. The authors are particularly grateful to Dr V.C. Farmer for providing them with a reprint of his recent publication and for his invaluable comments throughout the review process.

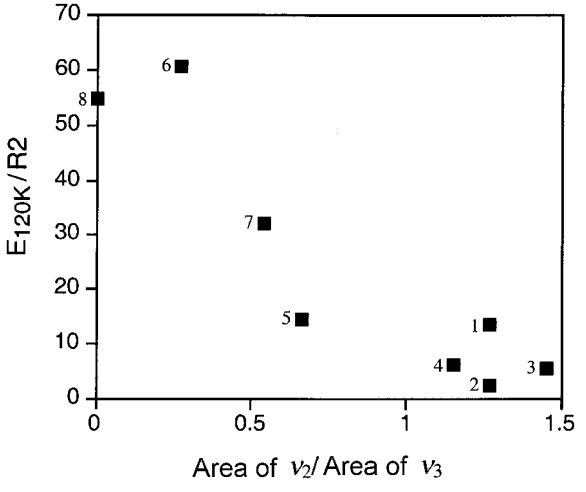

Figure 14. Relationships between the ratio of the disorder indexes, $E_{120K}/R2$, and $A\nu_2/A\nu_3$ for the well-characterized reference kaolinites (see Table 1 for an explanation of E_{120K} and R2, and for the numbers attached to the filled squares).

REFERENCES

Allard, T. (1994) La kaolinite: un dosimètre des rayonnements naturels. Application au traçage de migrations anciennes de radioéléments dans la géosphère. Ph.D. thesis, Université de Paris VII, Paris, France, 205 pp.

Ambrosi, J.-P. and Nahon, D. (1986) Petrological and geochemical differentiation of lateritic iron crust profiles. *Chemical Geology*, **57**, 371–393.

Angel, B.R., Jones, J.P.E. and Hall, P.L. (1974) Electron spin resonance studies of doped synthetic kaolinite. I. *Clay Minerals*, **10**, 247–255.

Balan, E., Allard, Th., Boizot, B., Morin, G. and Muller, J.-P. (1999) Structural Fe^{3+} in natural kaolinites: new insights from electron paramagnetic resonance spectra fitting at X and Q-band frequencies. *Clays and Clay Minerals,* **47**, 605–616.

Barrios, J., Plançon, M., Cruz, I. and Tchoubar, C. (1977) Qualitative and quantitative study of stacking faults in a hydrazine treated kaolinte – Relationship with the infrared spectra. *Clays and Clay Minerals,* **25**, 422–429.

Beauvais, A. (1991) Paléoclimats et dynamique d'un paysage cuirassé du Centrafrique. Morphologie, Pétrologie et Géochimie. Ph.D. thesis, Université de Poitiers, Poitiers, France, 317 pp.

Beauvais, A. (1999) Geochemical balance of lateritization processes and climatic signatures in weathering profiles overlain by ferricretes in Central Africa. *Geochimica et Cosmochimica Acta,* **63**, 3939–3957.

Beauvais, A. and Colin, F. (1993) Formation and transformation processes of iron duricrust systems in tropical humid environment. *Chemical Geology*, **106**, 77–151.

Beauvais, A. and Tardy, Y. (1991) Formation et dégradation des cuirasses ferrugineuses sous climat tropical humide, à la lisière de la forêt équatoriale. *Comptes Rendus de l'Académie des Sciences, Paris,* Séries II, **13**, 1539–1545.

Bell, V.A., Citro, V.R. and Hodge, G.D. (1991) Effect of pellet pressing on the infrared spectrum of kaolinite. *Clays and Clay Minerals,* **39**, 290–292.

Bish, D.L. (1993) Rietveld refinement of the kaolinite structure at 1.5 K. *Clays and Clay Minerals,* **41**, 738–744.

Brindley, G.W., Kao C.-C., Harrison, J.L., Lipsicas, M. and Raythatha, R. (1986) Relation between structural disorder and other characteristics of kaolinites and dickites. *Clays and Clay Minerals,* **34**, 239–249.

Cantinolle, P., Didier, P., Meunier, J.-D., Parron, C., Guendon, J.-L., Bocquier, G. and Nahon, D. (1984) Kaolinites ferrifères et oxyhydroxydes de fer et d'alumine dans les bauxites des Canonettes (S.E. de la France). *Clay Minerals*, **19**, 125–135.

Cases, J.-M., Liétard, O., Yvon, J. and Delon, J.-F. (1982) Etude des propriétés cristallochimiques, morphologiques, superficielles de kaolinites désordonnées. *Bulletin de Minéralogie*, **105**, 439–455.

Cruz-Cumplido, M., Sow, C. and Fripiat, J.J. (1982) Spectre infrarouge des hydroxyles, cristallinité et énergie de cohésion des kaolins. *Bulletin de Minéralogie*, **105**, 493–498.

Delineau, T., Allard, T., Muller, J.-P., Barres, O., Yvon, J. and Cases, J.-M. (1994) FTIR reflectance *vs.* EPR studies of structural iron in kaolinites. *Clays and Clay Minerals,* **42**, 308–320.

Didier, P., Nahon, D., Fritz, B. and Tardy, Y. (1983) Activity of water as a geochemical controlling factor in ferricretes. A thermodynamic model in the system kaolinite Fe-Al oxyhydroxides. *Sciences Geologiques,* **71**, 25–44.

Farmer, V.C. (1964) Infrared absorption of hydroxyls groups in kaolinite. *Science*, **145**, 1189–1190.

Farmer, V.C. (1974) *The Infrared Spectra of Minerals*. Monograph **4.** The Mineralogical Society, London, 539 pp.

Farmer, V.C. (1998) Differing effects of particle size and shape in the infrared and Raman spectra of kaolinite. *Clay Minerals*, **33**, 601–604.

Farmer, V.C. (2000) Transverse and longitudinal crystal modes associated with OH stretching vibrations in single crystals of kaolinite and dickite. *Spectrochimica Acta*, **56A**, 927–930.

Farmer, V.C. and Russell, J.D. (1964) The infrared spectra of layer silicates. *Spectrochimica Acta*, **20**, 1149–1173.

Frost, R.L. and Johansson, U. (1998) Combinations bands in the infrared spectroscopy of kaolins – a drift spectroscopic study. *Clays and Clay Minerals,* **46**, 466–477.

Frost, R.L. and Van der Gaast, S.J. (1997) Kaolinite hydroxyls – a Raman microscopy study. *Clay Minerals*, **32**, 471–484.

Gaite, J.-M., Ermakoff, P. and Muller, J.-P. (1993) Characterization and origin of two Fe^{3+} EPR spectra in kaolinite. *Physics and Chemistry of Minerals*, **20**, 242–247.

Gaite, J.-M., Ermakoff, P., Allard, Th. and Muller, J.-P. (1997) Paramagnetic Fe^{3+}: a sensitive probe for disorder in kaolinite. *Clays and Clay Minerals,* **45**, 496–505.

Giese, R.F., Jr. (1988) Kaolin minerals. Structures and stability. Pp. 29–66 in: *Hydrous Phyllosilicates* (S.W. Bailey, editor). Reviews in Mineralogy, **19**. Mineralogical Society of America, Washington, D.C.

Herbillon, A.J. (1980) Mineralogy of oxisols and oxic materials. Pp. 109–126 in: *Soils with Variable Charge* (B.K.G. Theng, editor). New Zealand Society of Soil Science, Wellington, New Zealand.

Hinckley, D.N. (1963) Variability in "crystallinity" values among the kaolin deposits of the coastal plain of Georgia and South Carolina. Pp. 229–235 in: *Proceedings of the 11th National Clay Conference, Ottawa* (A. Swineford, editor). Pergamon Press, New York.

Johansson, U., Holmgren, A., Forsling, W. and Frost, R. (1998) Isotopic exchange of kaolinite hydroxyl protons: a diffuse reflectance infrared Fourier transform spectroscopy study. *Analyst,* **123**, 641–645.

Johnston, C.T., Sposito, G. and Birge, R.R. (1985) Raman spectroscopy study of kaolinite in aqueous suspension. *Clays and Clay Minerals,* **33**, 483–489.

Johnston, C.T., Agnew, S.F. and Bish, D.L. (1990) Polarized single-crystal Fourier-transform infrared microscopy of Ouray dickite and Keokuk kaolinite. *Clays and Clay Minerals,* **38**, 573–588.

Johnston, C.T., Helsen, J., Schoonheydt, R.A., Bish, D.L. and Agnew, S.F. (1998) Single-crystal Raman spectroscopic study of dickite. *American Mineralogist*, **83**, 75–84.

Jones, J.P.E., Angel, B.R. and Hall, P.L. (1974) Electron spin resonance studies of doped synthetic kaolinite. II. *Clay Minerals*, **10**, 257–270.

Ledoux, R.L. and White, J.L. (1964) Infrared study of selective deuteration of kaolinite and halloysite at room temperature. *Science*, **145**, 47–49

Lombardi, G., Russell, J.D. and Keller, W.D. (1987) Compositional and structural variations in the size fractions of a sedimentary and a hydrothermal kaolin. *Clays and Clay Minerals,* **35**, 321–335.

Lucas, Y., Chauvel, A. and Ambrosi, J.-P. (1987) Processes of aluminium and iron accumulation in latosols developed on quartz-rich sediments from central Amazonia (Manaus, Brazil). Pp. 289–299 in: *Proceedings of the International Meeting on Geochemistry of the Earth Surface and Processes of Mineral formation, Granada, Spain* (R. Rodríguez-Clemente and Y. Tardy, editors). Madrid: Consejo Superior de Investigaciones Cientificas; Paris: Centre National de la Recherche Scientifique (CNRS).

Marquardt, D.W. (1963) An algorithm for least-squares estimation of nonlinear parameters. *Journal of the Society*

of Industrial Applied Mathematics, **11**, 431–441.
Meads, R.E. and Malden, P.S. (1975) Electron-spin resonance in natural kaolinites containing Fe^{3+} and other transition metal ions. *Clay Minerals*, **10**, 313–345.
Mendelovici, E., Yariv, S.H. and Villalba, R. (1979) Iron-bearing kaolinite in Venezuelan laterite. I. Infrared spectrosocopy and chemical dissolution evidence. *Clay Minerals*, **14**, 323–331.
Mestdagh, M.M., Vielvoye, L. and Herbillon, A.J. (1980) Iron in kaolinite: II. The relationship between kaolinite crystallinity and iron content. *Clay Minerals*, **15**, 1–13.
Mestdagh, M.M., Herbillon, A.J., Rodrique, L. and Rouxhet, P.G. (1982) Evaluation du rôle du fer structural sur la cristalinité des kaolinites. *Bulletin de Minéralogie*, **105**, 457–466.
Millot, G. (1970) *Geology of Clays: Weathering, Sedimentation, Geochemistry*. Springer, New York, 429 pp.
Muller, J.-P. and Bocquier, G. (1987) Textural and mineralogical relationships between ferruginous nodules and surrounding clayey matrices in a laterite from Cameroon. Pp. 186–194 in: *Proceedings of the International Clay Conference, Denver, 1985* (L.G. Schultz, H. van Olphen and F.A. Mumpton, editors). The Clay Minerals Society, Bloomington, Indiana.
Muller, J.-P. and Calas, G. (1989) Tracing kaolinites through their defect centers: kaolinite paragenesis in a laterite (Cameroon). *Economic Geology*, **84**, 694–707.
Muller, J.-P., Manceau, A., Calas, G., Allard, T., Ildefonse, Ph. and Hazemann, J.-L. (1995) Crystal chemistry of kaolinite and Fe-Mn oxides: relation with formation conditions of low temperature systems. *American Journal of Science*, **295**, 1115–1155.
Murray, H.H. (1988) Kaolin minerals: their genesis and occurrences. Pp. 67–90 in: *Hydrous Phyllosilicates* (S.W. Bailey, editor). Reviews in Mineralogy, **19.** Mineralogical Society of America, Washington, D.C.
Nahon, D. (1991) *Introduction to the Petrology of Soils and Chemical Weathering*. John Wiley, New York, 313 pp.
Parker, T.W. (1969) Classification of kaolinites by infrared spectroscopy. *Clay Minerals*, **8**, 19–35.
Petit, S. and Decarreau, A. (1990) Hydrothermal (200°C) synthesis and crystal chemistry of iron rich kaolinites. *Clay Minerals*, **25**, 181–196.
Plançon, A., Giese, R.F. and Snyder, R. (1988) The Hinckley index for kaolinites. *Clay Minerals*, **23**, 249–260.
Plançon, A., Giese, R.F., Snyder, R., Drits, V.A. and Bookin, A.S. (1989) Stacking faults in the kaolin-group minerals: defect structures of kaolinite. *Clays and Clay Minerals*, **37**, 203–210.
Prost, R., Dameme, A., Huard, E., Driard, J. and Leydecker, J.-P. (1989) Infrared study of structural OH in kaolinite, dickite, nacrite and poorly crystalline kaolinite at 5 to 600°K. *Clays and Clay Minerals*, **37**, 464–468.
Rengasamy, P. (1976) Substitution of iron and titanium in kaolinites. *Clays and Clay Minerals*, **24**, 264–266.
Rintoul, L. and Fredericks, P.M. (1995) Infrared microspectroscopy of bauxitic pisoliths. *Applied Spectroscopy*, **49**, 1608–1616.
Rouxhet, P.G., Samadacheata, N., Jacobs, H. and Anton, O. (1977) Attribution of the OH stretching bands of kaolinite. *Clay Minerals*, **12**, 171–179.
Tardy, Y. (1993) *Pétrologie des Latérites et des Sols Tropicaux*. Masson, Paris, 535 pp.
Van Olphen, H. and Fripiat, J.-J. (1979) *Data Handbook for Clay Minerals and other Non-metallic Minerals*. Pergamon Press, Oxford, UK, 346 pp.
Wiewióra, A., Wieckowski, T. and Sokolowska, A. (1979) The raman spectra of kaolinite subgroup minerals and of pyrophyllite. *Archiwum Mineralogiczne*, **135**, 5–14.

(*Received 3 January 2001; revised 9 November 2001; Ms. 511*)